

Simple microscopic model for magnetoelectric coupling in type-II antiferromagnetic multiferroics

L. Pili , R. A. Borzi , D. C. Cabra, and S. A. Grigera *Instituto de Física de Líquidos y Sistemas Biológicos (IFLYSIB), UNLP-CONICET, La Plata, Argentina and Departamento de Física, Facultad de Ciencias Exactas, Universidad Nacional de La Plata, La Plata, Argentina*

(Received 12 November 2021; revised 9 March 2022; accepted 9 March 2022; published 22 March 2022)

We present a simple two-dimensional model in which the lattice degrees of freedom mediate the interactions between magnetic moments and electric dipoles. This model reproduces basic features, such as a sudden electric polarization switch-off when a magnetic field is applied and the ubiquitous dimerized distortion patterns and magnetic $\uparrow\uparrow\downarrow\downarrow$ ordering, observed in several multiferroic materials of different composition. The list includes E-type manganites, RMnO_3 , nickelates such as YNiO_3 , and other materials under strain, such as TbMnO_3 . In spite of its simplicity, the model presented here captures the essence of the origin of multiferroicity in a large class of type-II multiferroics.

DOI: [10.1103/PhysRevB.105.094428](https://doi.org/10.1103/PhysRevB.105.094428)

I. INTRODUCTION

Multiferroic (MF) materials, those in which electric and magnetic degrees of freedom are coupled, are a subject of growing interest, not only for their potential technological applications but also because of the theoretical interest raised by the different unusual properties and effects discovered over the last years [1–5]. Of interest in regard to technological applications is the possibility of using multiferroicity for low-energy switching in data storage devices that could lead to future-generation ultralow-energy electronics. Coupling between the magnetic and ferroelectric orders could allow for bit imprinting by an *electric* rather than magnetic field [6–8].

Among the large family of MF materials known today, there is a special class, dubbed *improper type-II MFs*, which are distinguished by the fact that the magnetic and ferroelectric orders occur simultaneously through a cooperative transition (see, e.g., Refs. [9–11]). An important subclass of these materials is that in which the magnetic order is collinear at low temperatures and consists of an arrangement of spins following a period-4 pattern $\uparrow\uparrow\downarrow\downarrow$ in one, two, or three directions of the crystal, which we will refer to as *uudd*.

A nonexhaustive list of materials in this special class includes (i) a large group of nickelates, which show first a metal-insulator transition involving a structural change, followed by a paramagnet to type-E antiferromagnetic phase, with magnetic *uudd* ordering along the three crystal directions [12,13]; (ii) manganites, which are believed to exhibit both ferroelectric and antiferromagnetic transitions and in some cases, e.g., in HoMnO_3 , a magnetic *uudd* ordering (also type E) simultaneous with a structural change [14–16]; and (iii) double perovskites such as $\text{Yb}_2\text{CoMnO}_6$ [17], Y_2CoMnO_6 [18], $\text{Lu}_2\text{MnCoO}_6$ [19,20], $\text{Er}_2\text{CoMnO}_6$ [21], and R_2NiMnO_6 ($R = \text{Pr, Nd, Sm, Gd, Tb, Dy, Ho, Er}$), where a giant magnetoelectric effect has been reported [22]. Last but not least, the iron selenide BaFe_2Se_3 , which becomes a superconductor under pressure [23,24], shows *uudd* magnetic ordering in 2×2

plaquettes along two-leg ladders and is hence best modeled in one dimension, along the lines of Refs. [25,26].

Motivated by these multiple observations, we present a minimal model where a simple mechanism stabilizes the ubiquitous lattice dimerization and *uudd* spin ordering. In our model, local dipoles arise from spontaneous distortions of the crystal lattice, which are in turn stabilized by the magnetoelastic coupling and affected by the consequent electric (dipole-dipole) interactions. A related one-dimensional (1D) model proposal, which reproduces the basic phenomenology of 1D materials, has been recently analyzed in Refs. [25,26]. Related “exchange-striction” mechanisms to explain MF behavior in different classes of materials have been proposed and studied (see, e.g., Ref. [27]).

In a previous paper [28], two of the authors studied a magnetoelastic two-dimensional Ising model in which three main phases were in competition: a ferromagnetic (FM) or antiferromagnetic (AFM) phase on the undistorted square lattice, a so-called plaquette or checkerboard (CB) phase, and the stripe (ST) phase. The latter corresponds to an E-type *uudd* magnetic ordering along the two principal crystal directions. The deformation is only stable when it involves a sign reversal on some of the exchange constants [see Figs. 1(b) and 1(c)]. These same two magnetoelastic phases have been also studied in the quantum spin-Peierls case [29] in a square lattice. It was shown in Ref. [28] that for phenomenologically reliable couplings the CB phase is always lower in energy. Here, we add two ingredients to this purely magnetoelastic model. On the one hand, lattice deformations drive the setup of electric dipole moments via distortions of the charge environment. On the other hand, we take into account the dipole-dipole interactions resulting from these moments. Interestingly, we observe that these electric dipolar interactions can alter the relative values of the ground-state energies of these phases, turning the ST or *uudd* phase—the one relevant to the experiments listed above—into the stable one even within this classical framework. Magnetoelectric coupling and its relation to lattice

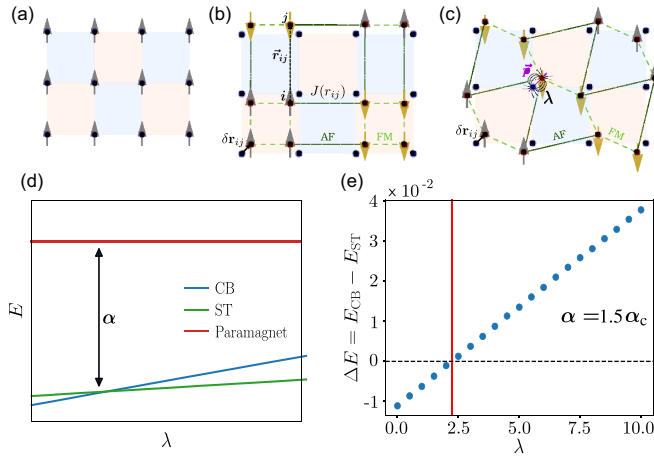


FIG. 1. Interaction terms and phases. Aside from the paramagnetic phase, three ordered states are relevant to this study. Magnetic and elastic degrees of freedom are taken on an equal footing in our model, but the names chosen refer to spin configurations. (a) Ordered Ising state (ferromagnetic in the example pictured). For relatively small values of the magnetoelastic coupling α , this is the preferred spin configuration. Distortions average zero in this state. (b) Checkerboard phase and (c) stripe phase. If the magnetoelastic coupling constant α is bigger than α_c , it is favorable to deform the lattice. These deformations imply a dipolar electric moment $\mathbf{p}_i = \gamma_i \delta \mathbf{r}_i$, represented here by pairs of colored circles. (d) Dipolar interactions, with an energy scale given by λ , do not affect the FM or the paramagnet, but change the energy balance between the ST and CB phases. (e) As shown here for an example with $\alpha = 1.5\alpha_c$, and with $\gamma_i = 1, 2$ for odd and even sites, respectively, the ST becomes the ground state of the system above $\lambda_c = 2.45$.

deformations have been discussed in other contexts, such as in BiFeO₃ [30,31], where magnetic orderings are of a cycloid type. In such cases, the origin of the polarization in relation to the magnetic ordering has a different origin from the one we discuss in this paper (see, e.g., Refs. [32,33]).

We show that the magnetoelectric coupling is quite effective. Crucially, it leads to a sharp switch-off of the spontaneous polarization as a function of the applied magnetic field, in concurrence with a metamagnetic transition. These simultaneous transitions have been observed in a wide variety of materials, such as Er₂CoMnO₆ [21], Lu₂CoMnO₆ [19,34], and R₂V₂O₇ (R = Ni, Co) [35]. The effect is also observed in some noncollinear cases, such as TbMnO₃, which shows gigantic magnetoelectric and magnetocapacitance effects [36]. Interestingly enough, this material can be driven into an *uudd* state by epitaxial strain [37]. Our model and its predictions could be tested in magnetic field experiments that should allow one to observe the increase in the magnetization and a simultaneous sizable drop in the electric polarization. This could be important, e.g., for some nickelates for which the magnetic structure is still under debate [38]. Indeed, in Ref. [39], using recently synthesized single crystals, the first experimental evidence of the possible connection between the *uudd* ordering and a bulk polarization has been given. Magnetization experiments using these samples would be the next step to further confirm our predictions.

II. THE MODEL

This Ising model is based on the so-called *Einstein site phonon spin model* [40], which considers a coupling between magnetic and elastic degrees of freedom. In it, the sites have displacements given by a set of independent harmonic oscillators. This assumes that the most important lattice distortion contribution is coming from optical phonons, which is a reasonable choice given that in real materials the active magnetic lattice is usually a sublattice of a more complex crystal structure. The model presented here incorporates electrical properties by assuming that each site displacement implies the formation of a dipolar electric moment; dipole-dipole interactions are then considered up to first-nearest neighbors. As we will discuss afterwards, this does not affect our results, and it considerably speeds up our simulations, which follow the simultaneous evolution of two sets of coupled degrees of freedom. The Hamiltonian is given by

$$\frac{\mathcal{H}}{|J_0|} = \sum_{\langle i,j \rangle} J(r_{ij}) S_i S_j + \frac{K_e}{2} \sum_i (\delta \mathbf{r}_i)^2 + \lambda \sum_{\langle i,j \rangle} [\mathbf{p}_i \cdot \mathbf{p}_j - 3(\mathbf{r}_{ij}^0 \cdot \mathbf{p}_j)(\mathbf{r}_{ij}^0 \cdot \mathbf{p}_i)] + \mathcal{H}_{\text{field}}, \quad (1)$$

where S_i stands for an Ising-type spin pointing along the [01] crystal direction ($S_i = \pm 1$) at position \mathbf{r}_i measured in units of the cell constant. $\mathbf{r}_{ij} = \mathbf{r}_i - \mathbf{r}_j$ are the relative position vectors of different spins. We call $\delta \mathbf{r}_i \equiv \mathbf{r}_i - \mathbf{r}_i^0$ the site displacement and $\delta r_{ij} \equiv (\mathbf{r}_{ij} - \mathbf{r}_{ij}^0)$ the distance change between sites [see Figs. 1(b) and 1(c)]. The distance-dependent [41] exchange constant is given by

$$J(r_{ij}) = \text{sgn}(J_0) [1 - \alpha \hat{e}_{ij} \cdot \delta \mathbf{r}_{ij}]. \quad (2)$$

Here, α is the magnetoelastic coupling, and \hat{e}_{ij} is the unit vector pointing from site i to site j . The electric dipole moment at site i is given by $\mathbf{p}_i = \gamma_i \delta \mathbf{r}_i$. The proportionality constant, γ_i , can be site dependent if the system is composed of sublattices with different ionic charges. The sign function allows for the possibility of starting either with a ferromagnetic phase (the general assumption here) or with an antiferromagnetic one. Being that the lattice is bipartite, the results can be mapped by performing a sign reversal of the spins in one sublattice.

External magnetic and electric fields are taken into account by the term

$$\mathcal{H}_{\text{field}} = -B \sum_i S_i - \sum_i \mathbf{E} \cdot \mathbf{p}_i, \quad (3)$$

where B points trivially along the y direction and E points along the diagonal directions of the lattice.

To simulate the elastic distortions, we consider polar coordinates (ρ, θ) to describe each $\delta \mathbf{r}_i$. The angle θ is treated as in a clock model of 360 equally spaced angles, and the displacement ρ is chosen randomly in a distribution from 0 to a temperature-dependent maximum $\delta_{\text{max}}(T)$. The use of the latter has no impact on the results obtained from the simulation; it is introduced as a way to optimize speed by avoiding the proposal of extremely unlikely moves at low temperatures [28].

In accordance with the spirit of the model, the magnetic and elastic degrees of freedom are treated simultaneously in

the Monte Carlo simulations. We follow the method introduced in Ref. [28]. Each step of the simulation is split into elastic and magnetic moves. The simulation assumes that the relaxation times of the magnetic degrees are much shorter than those of the elastic degrees and hence each elastic move is done with a relaxed magnetic configuration. The algorithm proceeds as follows.

We perform P elastic Monte Carlo steps (MCSs) consisting of the following.

- (i) Choose a random site.
- (ii) Propose a move by picking at random an angle and a displacement (from 0 to δ_{\max}).
- (iii) Calculate the exchange constants for the proposed spatial configuration.
- (iv) Calculate the total energy of the system (magnetic + elastic) and accept or reject the move according to the Metropolis algorithm.
- (v) Make Q magnetic moves; each move consists of the following: (a) Flip one spin at random, (b) calculate the change in magnetic energy, (c) accept or reject according to the Metropolis algorithm, and (d) repeat steps (a)–(c) until each spin has been chosen at least once on average.
- (vi) Repeat steps (i)–(v) until each site has been chosen at least once on average.

The results are independent of the precise choice of the ratio P/Q . We have used square lattices with L from 4 to 16 and typically with 10^6 elastic MCSs for equilibration and another 10^6 site MCSs for acquiring data. The figures in this paper are all for $L = 16$.

III. RESULTS

A. $\gamma_i = 0$: Purely magnetoelastic system

The magnetoelastic phase diagram of the model in the absence of any polarization effects has been studied in Ref. [28]. As the magnetoelastic coupling α is increased, the critical temperature of the ordered FM or AFM Ising phase decreases steadily, reaching $T = 0$ at a critical coupling $\alpha_c = \sqrt{K_e/2}$, above which the system goes through a simultaneous magnetic and structural transition. The ground state becomes a *checkerboard* of ferromagnetic clusters, aligned antiferromagnetically [see Fig. 1(b)]. The critical temperature of the CB phase increases with increasing α . For values of α slightly above α_c there is another phase with long-range *uudd* order, the ST state, with energy comparable to the ground state. This state, pictured in Fig. 1(c), consists of diagonal ferromagnetic stripes aligned antiferromagnetically. While the CB state is the ground state, the energetic proximity of the stripe state means that additional interactions might easily reverse the situation. As we will see, this is the effect of electric dipolar interactions.

B. $\gamma_i \neq 0$: Multiferroicity

When $\gamma_i \neq 0$, electric dipole moments are developed that are proportional to the local site displacements. We begin by analyzing the simplest (homogeneous) case, i.e., $\gamma_i = \gamma$ for all i . In the paramagnetic or in the FM or AFM ordered phases this is irrelevant: Their minimum energy is achieved without distorting the square lattice. This is no longer true for $\alpha > \alpha_c$, and as can be seen in Figs. 1(b) and 1(c), both the checker-

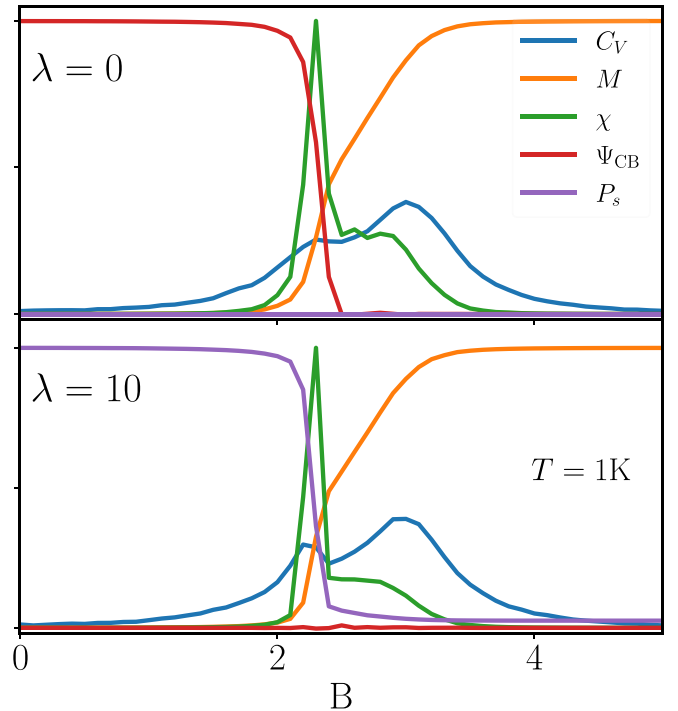


FIG. 2. Effect of the magnetic field on charge and magnetic degrees of freedom (case of homogeneous charge distribution $\gamma_i = \gamma$). Susceptibility peaks and the first peak in C_V coincide with the abrupt fall in P and the rise in M . The behavior is similar for both λ (i.e., for both ground states). In both cases, $\alpha = 1.5\alpha_c$. The rise in M is smooth and goes through an intermediate step marked by peaks in the specific heat.

board and the stripe states develop electric moments at every site, albeit with different configurations. When the dipolar interaction between these moments, proportional to λ , is taken into account to first-nearest neighbors, the balance between the energies of the CB and ST states changes. This is plotted in Fig. 1(d) for a fixed value of $\alpha > \alpha_c$. While the paramagnetic phase is trivially unaffected, the energy of both the CB and the ST phases grows linearly, with different slopes for each case. As shown in Fig. 1(d), there is a critical λ_c above which the ST phase becomes the ground state of the system. The role of the dipolar interaction is merely to select the ground state and does not alter the nature of the states themselves, which is determined by the (much stronger) magnetoelastic term. We checked that this perturbation selects the ST state for any interaction range. It follows that further neighbors in this calculation are not necessary unless one is interested in defining fine details of the resulting phase diagram [42].

For $\lambda > \lambda_c$ the ground state is a stripe phase. If $\gamma_i \neq 0$ is equal for all i , the order in the ST phase is antiferroelectric, since the sum of the displacements cancels out. The magnetic and electric dipole directions are not correlated with each other: The orientation of one does not determine the other.

There is a simple and physically sensible way in which a nonzero bulk polarization can arise in this model. A common type of crystal is composed of two interpenetrated square sublattices of different ions. If the polarizability of these sites is different, which can be easily taken into account in the model

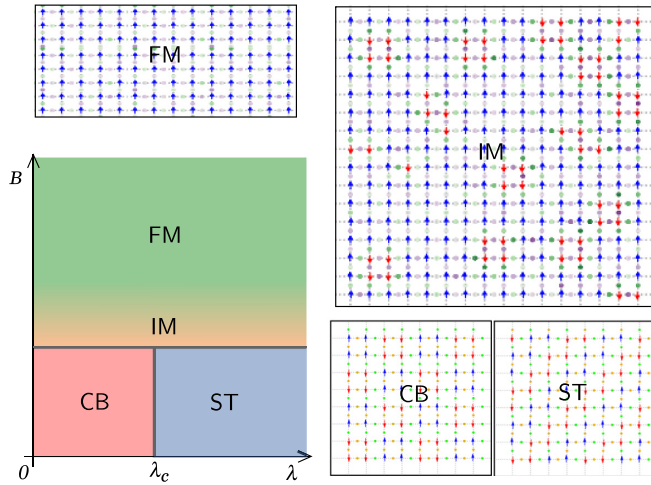


FIG. 3. B - λ phase diagram. For low fields the ground state of the system transitions from a checkerboard (CB), below λ_c , to a stripe phase (ST). As the field is increased, both the CB and ST states transition into a ferromagnet (FM) going through an intermediate state (IM) where the system is mostly ordered ferromagnetically, with some remnants of the low-field phases in the form of aligned clusters that oppose the magnetic field direction. The snapshot here represents one of the many possible spin and structural configurations taken by the system.

by making γ_i different in each sublattice, the ground state is not affected [see Fig. 1(e)], and there is a net polarization of the whole system (see inset of Fig. 4).

C. The effect of an external magnetic field

For $\alpha > \alpha_c$, both above and below λ_c , the magnetic ground states are different forms of antiferromagnetism. An external magnetic field eventually drives the system into a homogeneous FM state. Figure 2 shows the behavior of the magnetization, the magnetic susceptibility, and the specific heat as a function of the externally applied magnetic field both below λ_c (top panel, $\lambda = 0$) and above λ_c (bottom panel, $\lambda = 10$). In the first case, the magnetic ground state is a CB, and its order parameter Ψ_{CB} (see Appendix A) is also shown. In the second case, where the ground state is a ST, it is the staggered polarization P_s that is plotted as a function of the field. As shown in the figure, the behavior of the system is very similar regardless of the ground state: The antiferromagnetic state with $M = 0$ is preserved for low fields and eventually gives way to the FM state through a metamagnetic transition. The field at which this transition starts is very similar for both cases, which is to be expected, given the subtle energy difference between both magnetic ground states. There is a structure at the transition, evidenced as a double peak in the specific heat and as a peak and shoulder in the magnetic susceptibility.

The B - λ phase diagram can be simply sketched (Fig. 3): At low fields there is a transition between the CB and ST states as a function of λ . As the field is increased, the system polarizes into a FM state going through an intermediate state (IM), the existence of which is marked by the two peaks in the specific heat. Snapshots of the different phases, also shown in Fig. 3,

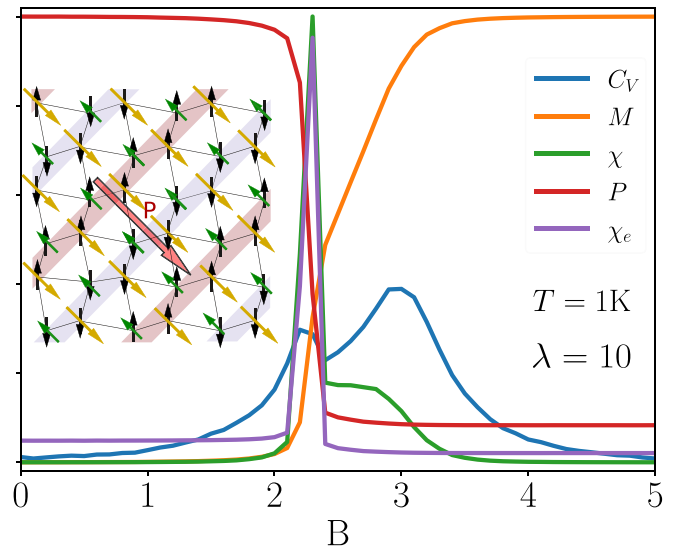


FIG. 4. Effect of the magnetic field on charge and magnetic degrees of freedom (nonhomogeneous charge distribution γ_i). In this case (sketched in the inset), where there are two sublattices with different charges, the system has a nonzero homogeneous polarization P at low fields. As in the case with $\gamma_i = \gamma$, the transition towards the high-field state is also marked by an intermediate phase.

give further information about the intermediate state: Here, the system is mostly ordered ferromagnetically but retains some remnants of the low-field phases in the form of aligned clusters that oppose the magnetic field direction.

The effect of introducing a nonhomogeneous γ_i by making γ_i different in two sublattices (as sketched in the inset of Fig. 4) leaves unchanged the overall behavior of the system as a function of magnetic field (Fig. 4). The crucial difference, in terms of experimental observables, is that in this case the system switches from a homogeneous $P \neq 0$ and $M = 0$ at low fields, to a negligible polarization $P \approx 0$ and a saturated $M \neq 0$ at high fields. The peaks in $\chi_M = dM/dB$ and $\chi_e = dP/dB$ coincide almost exactly. In this way the model reproduces the polarization switch-off observed in many experimental systems [19,21,34–36].

D. Scattering signatures

The ST and CB phases described before have signatures in scattering experiments, both in neutron scattering (the spin channel), coming from the different long-range ordered magnetic structures, and in x-ray scattering (the charge channel) as a consequence of their characteristic distortion patterns. These experimentally accessible characteristics can be calculated from the Monte Carlo simulations (see Appendix B).

Figure 5 shows the structure factors in the spin channel (left panels) and diffuse charge channel (right panels) for the ST phase (upper panels) and the CB phase (lower panels). As expected, for both channels, the stripe phase shows C_2 symmetry, while the checkerboard phase retains the C_4 symmetry of the lattice (albeit with a different unit cell).

IV. SUMMARY AND CONCLUSIONS

In this paper we present what is probably the simplest possible model that reproduces the basic features observed

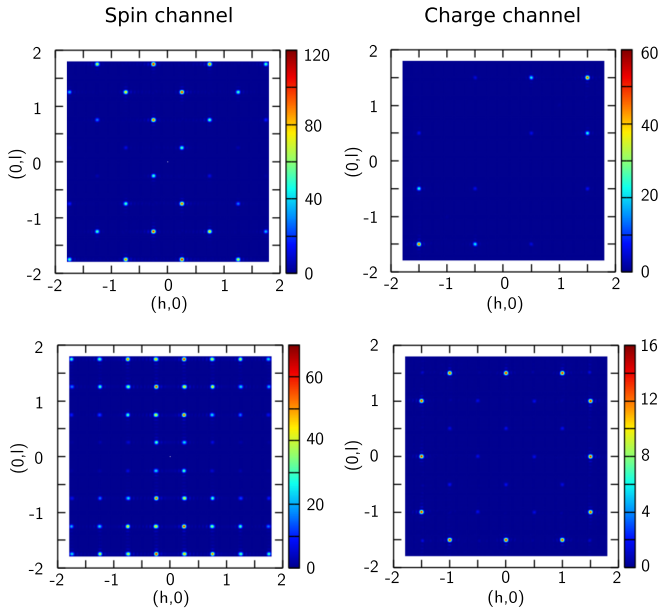


FIG. 5. Signatures in scattering experiments. Structure factors in the spin channel (left panels) and diffuse charge channel, associated with the displaced charges (right panels). The stripe phase (upper panels) shows C_2 symmetry in both channels, while the checkerboard phase (lower panels) retains the C_4 symmetry of the lattice.

in several multiferroic materials, such as E-type manganites, $RMnO_3$, nickelates such as $YNiO_3$, double perovskites, and other materials under strain, such as $TbMnO_3$. The model, based on the Einstein site phonon spin model, is a nearest-neighbor Ising model on a square lattice that adds coupling between magnetic and elastic degrees of freedom. The latter has two effects: First, it alters the local exchange interaction, and second, it gives rise to electric dipole moments, which in turn interact with a nearest-neighbor dipolar term. The presence of these two interactions changes the ground state of the system from the usual FM or AFM ordered state (depending on the sign of J) to a striped state where FM and AFM couplings coexist, with magnetic $uudd$ ordering, and where a nonzero polarization can develop. An applied magnetic field eventually switches off the electric polarization, driving the system into an ordered FM state through a metamagnetic transition.

The model presented here captures the essence of the origin of multiferroicity in a large class of type II multiferroics and given its simplicity is a promising toy model to further investigate these phenomena. Understanding the role of lattice distortions in the magnetoelastic coupling would also provide a useful guide to experiments under tensile strain and film depositions on mismatched substrates.

ACKNOWLEDGMENTS

We would like to acknowledge discussions with M. Medarde, M. Picco, and R. Santachiara and financial support from the Agencia Nacional de Promoción Científica y Tecnológica (ANPCyT) through PICTs 2017-2347 and

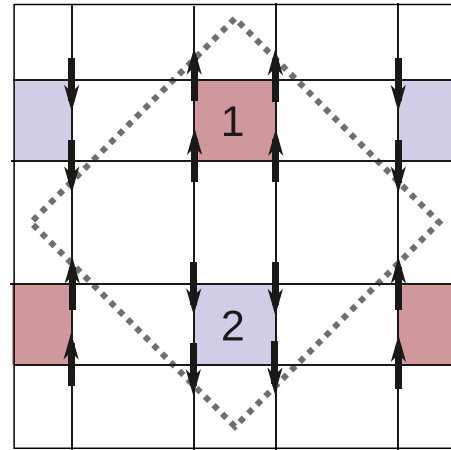


FIG. 6. Unit cell and labels used for the calculation of Φ_{CB} .

2015-0813 and from the Consejo Nacional de Investigaciones Científicas y Técnicas (CONICET) through PIP 2015-0446 and 2021-1146.

APPENDIX A: DEFINITION OF THE CB ORDER PARAMETER

We use the order parameter for the checkerboard phase as defined in Ref. [28]. For this we use a unit cell such as the one shown in Fig. 6. The index j is defined that runs over all squares in the lattice counting as odd and even the squares marked with 1 and 2, respectively, in the picture, and an index a is defined that runs over the spins in the squares. There are four possible degeneracies of the ground state (plus time reversal), corresponding to where the colored squares are set in the unit cell. We then define an order parameter Φ_{CB} that is the sum over the four possibilities,

$$\Phi_{CB} = 1/N \sum_{m=0}^4 (-1)^m |\Phi_m|, \quad (A1)$$

where

$$\Phi_m = \sum_{j=1}^{N/4} \sum_{a=1}^4 (-1)^j e^{i\phi_a^m} \sigma_a^j. \quad (A2)$$

Here, σ_a^j are Ising-spin variables that can take the values ± 1 , N is the total number of spins, and ϕ_a^m are the phase factors for the spin that take into account the four possible degeneracies: $\phi^1 = \pi(0, 0, 0, 0)$, $\phi^2 = \pi(1, 0, 1, 0)$, $\phi^3 = \pi(1, 1, 0, 0)$, and $\phi^4 = \pi(1, 0, 0, 1)$.

APPENDIX B: CALCULATION OF THE NEUTRON STRUCTURE FACTOR

The simulated neutron structure factors have been calculated following the expression

$$I^{\text{spin}}(\mathbf{k}) = \frac{1}{N} \sum_{ij} \langle S_i S_j \rangle (\boldsymbol{\mu}_i^\perp \cdot \boldsymbol{\mu}_j^\perp) e^{i\mathbf{k} \cdot \mathbf{r}_{ij}},$$

where i and j sweep the square lattice, N is the number of spins, and $\langle \dots \rangle$ represents the thermal average (in this

case, that of the product of spins at sites i, j). The spin quantization directions are given by $\{\hat{\mu}_i\}$ (parallel to the $\langle 01 \rangle$ directions). Then, μ_i^\perp is the component of $\hat{\mu}_i$ of the spin $S_i = S_i \hat{\mu}_i$ at site i perpendicular to the scattering wave vector \mathbf{k} :

$$\mu_i^\perp = \hat{\mu}_i - \left(\hat{\mu}_i \cdot \frac{\mathbf{k}}{|\mathbf{k}|} \right) \frac{\mathbf{k}}{|\mathbf{k}|}. \quad (\text{B1})$$

For the *diffuse* structure factor associated with the displaced ions, assuming an atomic form factor of unity, we

calculated

$$I^{\text{el.-dip.}}(\mathbf{k}) = \frac{2}{N} \sum_{\alpha\beta} \langle [e^{i\mathbf{k}\cdot\delta\mathbf{r}_\alpha} - q^{\text{av}}(\mathbf{k})] \times [e^{-i\mathbf{k}\cdot\delta\mathbf{r}_\beta} - q^{\text{av}}(\mathbf{k})] \rangle e^{i\mathbf{k}\cdot\mathbf{r}_{\alpha\beta}},$$

where $q^{\text{av}}(\mathbf{k}) = \langle e^{i\mathbf{k}\cdot\delta\mathbf{r}_\alpha} \rangle$ is an average, k -dependent “charge” in the perfect square lattice.

In both cases we have thermally averaged over sets composed of 500–1000 independent configurations for a system size $L = 16$.

- [1] W. Eerenstein, N. Mathur, and J. F. Scott, *Nature (London)* **442**, 759 (2006).
- [2] N. Hur, I. K. Jeong, M. F. Hundley, S. B. Kim, and S.-W. Cheong, *Phys. Rev. B* **79**, 134120 (2009).
- [3] S. Lee, A. Pirogov, M. Kang, K.-H. Jang, M. Yonemura, T. Kamiyama, S.-W. Cheong, F. Gozzo, N. Shin, H. Kimura, Y. Noda, and J.-G. Park, *Nature (London)* **451**, 805 (2008).
- [4] S. Dong, J.-M. Liu, S.-W. Cheong, and Z. Ren, *Adv. Phys.* **64**, 519 (2015).
- [5] M. Fiebig, T. Lottermoser, D. Meier, and M. Trassin, *Nat. Rev. Mater.* **1**, 16046 (2016).
- [6] M. M. Vopson, *Crit. Rev. Solid State Mater. Sci.* **40**, 223 (2015).
- [7] J. Wang, *Multiferroic Materials: Properties, Techniques, and Applications* (CRC, Boca Raton, FL, 2016).
- [8] T. Hu and E. Kan, *Wiley Interdiscip. Rev.: Comput. Mol. Sci.* **9**, e1409 (2019).
- [9] J. Van Den Brink and D. I. Khomskii, *J. Phys.: Condens. Matter* **20**, 434217 (2008).
- [10] D. Khomskii, *Physics* **2**, 20 (2009).
- [11] S.-W. Cheong and M. Mostovoy, *Nat. Mater.* **6**, 13 (2007).
- [12] M. L. Medarde, *J. Phys.: Condens. Matter* **9**, 1679 (1997).
- [13] S. Catalano, M. Gibert, J. Fowlie, J. Iniguez, J.-M. Triscone, and J. Kreisel, *Rep. Prog. Phys.* **81**, 046501 (2018).
- [14] I. A. Sergienko, C. Şen, and E. Dagotto, *Phys. Rev. Lett.* **97**, 227204 (2006).
- [15] S. Dong, R. Yu, S. Yunoki, J.-M. Liu, and E. Dagotto, *Eur. Phys. J. B* **71**, 339 (2009).
- [16] M. Lilienblum, T. Lottermoser, S. Manz, S. M. Selbach, A. Cano, and M. Fiebig, *Nat. Phys.* **11**, 1070 (2015).
- [17] J. Blasco, J. L. García-Muñoz, J. García, J. Stankiewicz, G. Subías, C. Ritter, and J. Rodríguez-Velamazán, *Appl. Phys. Lett.* **107**, 012902 (2015).
- [18] J. K. Murthy, K. D. Chandrasekhar, H. Wu, H. Yang, J.-Y. Lin, and A. Venimadhav, *EPL (Europhys. Lett.)* **108**, 27013 (2014).
- [19] S. Chikara, J. Singleton, J. BOWLAN, D. A. Yarotski, N. Lee, H. Y. Choi, Y. J. Choi, and V. S. Zapf, *Phys. Rev. B* **93**, 180405(R) (2016).
- [20] J. T. Zhang, X. M. Lu, X. Q. Yang, J. L. Wang, and J. S. Zhu, *Phys. Rev. B* **93**, 075140 (2016).
- [21] M. K. Kim, J. Y. Moon, S. H. Oh, D. G. Oh, Y. J. Choi, and N. Lee, *Sci. Rep.* **9**, 5456 (2019).
- [22] H. Y. Zhou, H. J. Zhao, W. Q. Zhang, and X. M. Chen, *Appl. Phys. Lett.* **106**, 152901 (2015).
- [23] S. Dong, J.-M. Liu, and E. Dagotto, *Phys. Rev. Lett.* **113**, 187204 (2014).
- [24] X. Liu, C. Ma, C. Hou, Q. Chen, R. Sinclair, H. Zhou, Y. Yin, and X. Li, *EPL (Europhys. Lett.)* **126**, 27005 (2019).
- [25] D. C. Cabra, A. O. Dobry, C. J. Gazza, and G. L. Rossini, *Phys. Rev. B* **100**, 161111(R) (2019).
- [26] D. C. Cabra, A. O. Dobry, C. J. Gazza, and G. L. Rossini, *Phys. Rev. B* **103**, 144421 (2021).
- [27] G. S. Jeon, J.-H. Park, J. W. Kim, K. H. Kim, and J. H. Han, *Phys. Rev. B* **79**, 104437 (2009).
- [28] L. Pili and S. A. Grigera, *Phys. Rev. B* **99**, 144421 (2019).
- [29] J. Sirker, A. Klumper, and K. Hamacher, *Phys. Rev. B* **65**, 134409 (2002).
- [30] D. Albrecht, S. Lisenkov, W. Ren, D. Rahmedov, I. A. Kornev, and L. Bellaiche, *Phys. Rev. B* **81**, 140401(R) (2010).
- [31] D. Rahmedov, D. Wang, J. Íñiguez, and L. Bellaiche, *Phys. Rev. Lett.* **109**, 037207 (2012).
- [32] H. Katsura, N. Nagaosa, and A. V. Balatsky, *Phys. Rev. Lett.* **95**, 057205 (2005).
- [33] I. A. Sergienko and E. Dagotto, *Phys. Rev. B* **73**, 094434 (2006).
- [34] S. Yáñez-Vilar, E. D. Mun, V. S. Zapf, B. G. Ueland, J. S. Gardner, J. D. Thompson, J. Singleton, M. Sánchez-Andújar, J. Mira, N. Biskup, M. A. Senaris-Rodríguez, and C. D. Batista, *Phys. Rev. B* **84**, 134427 (2011).
- [35] R. Chen, J. F. Wang, Z. W. Ouyang, Z. Z. He, S. M. Wang, L. Lin, J. M. Liu, C. L. Lu, Y. Liu, C. Dong, C. B. Liu, Z. C. Xia, A. Matsuo, Y. Kohama, and K. Kindo, *Phys. Rev. B* **98**, 184404 (2018).
- [36] T. Kimura, T. Goto, H. Shintani, K. Ishizaka, T. Arima, and Y. Tokura, *Nature (London)* **426**, 55 (2003).
- [37] K. Shimamoto, S. Mukherjee, S. Manz, J. S. White, M. Trassin, M. Kenzelmann, L. Chapon, T. Lippert, M. Fiebig, C. W. Schneider, and C. Niedermayer, *Sci. Rep.* **7**, 44753 (2017).
- [38] I. Ardizzone, J. Teyssier, I. Crassee, A. B. Kuzmenko, D. G. Mazzone, D. J. Gawryluk, M. Medarde, and D. Van Der Marel, *Phys. Rev. Res.* **3**, 033007 (2021).
- [39] Y. M. Klein, M. Kozłowski, A. Linden, P. Lacorre, M. Medarde, and D. J. Gawryluk, *Cryst. Growth Des.* **21**, 4230 (2021).
- [40] F. Wang and A. Vishwanath, *Phys. Rev. Lett.* **100**, 077201 (2008).
- [41] This dependence can also be thought of as a parametrization of an angle-dependent interaction, when it is mediated by a nonmagnetic ion (as in HoMnO₃).
- [42] Fixing the displacements in their low-temperature-high- α values $\delta r_i = \delta r(\pm 1, \pm 1)$, the dipolar electric energy as a function of the range saturates rapidly for both distorted phases. The dipolar energy varies by less than 2% of its asymptotic value when the interaction range goes above the tenth-nearest neighbor.